Tumor protein D54 binds intracellular nanovesicles via an extended amphipathic region

Antoine Reynaud, Maud Magdeleine, Amanda Patel, Anne-Sophie Gay, Delphine Debayle, Sophie Abelanet, Bruno Antonny

JBC RESEARCH ARTICLE

Tumor protein D54 binds intracellular nanovesicles *via* an extended amphipathic region

Received for publication, January 27, 2022, and in revised form, June 7, 2022 Published, Papers in Press, June 14, 2022,
https://doi.org/10.1016/j.jbc.2022.102136

Antoine Reynaud, Maud Magdeleine, Amanda Patel, Anne-Sophie Gay, Delphine Debayle, Sophie Abelanet, and Bruno Antonny*

From the Université Côte d'Azur et CNRS, Institut de Pharmacologie Moléculaire et Cellulaire, Valbonne, France

Edited by Phyllis Hanson

Tumor protein D54 (TPD54) is an abundant cytosolic protein that belongs to the TPD52 family, a family of four proteins (TPD52, 53, 54, and 55) that are overexpressed in several cancer cells. Even though the functions of these proteins remain elusive, recent investigations indicate that TPD54 binds to very small cytosolic vesicles with a diameter of ca. 30 nm, half the size of classical (*e.g.*, COPI and COPII) transport vesicles. Here, we investigated the mechanism of intracellular nanovesicle capture by TPD54. Bioinformatical analysis suggests that TPD54 contains a small coiled-coil followed by four amphipathic helices (AH1-4), which could fold upon binding to lipid membranes. Limited proteolysis, CD spectroscopy, tryptophan fluorescence, and cysteine mutagenesis coupled to covalent binding of a membrane-sensitive probe showed that binding of TPD54 to small liposomes is accompanied by large structural changes in the amphipathic helix region. Furthermore, site-directed mutagenesis indicated that AH2 and AH3 have a predominant role in TPD54 binding to membranes both in cells and using model liposomes. We found that AH3 has the physicochemical features of an amphipathic lipid packing sensor (ALPS) motif, which, in other proteins, enables membrane binding in a curvature-dependent manner. Accordingly, we observed that binding of TPD54 to liposomes is very sensitive to membrane curvature and lipid unsaturation. We conclude that TPD54 recognizes nanovesicles through a combination of ALPS-dependent and ALPS-independent mechanisms.

In cells, transport vesicles are produced from membrane-bound organelles by vesicular coat complexes, which self-assemble at the organelle surface into spherical shells to promote the budding of coated vesicles (1, 2). The best characterized protein coats are COPII, COPI, AP1-clathrin, and AP2-clathrin, which promote vesicle budding from the endoplasmic reticulum, Golgi apparatus (GA), *trans*-Golgi network (TGN), and plasma membrane, respectively. These different coats and the corresponding classes of vesicles have been abundantly studied over the last decades, notably as regards to the mechanisms of coat assembly, coat structure, vesicular content in cargoes, and associated diseases (3, 4). Investigations by electron microscopy both *in situ* and from reconstituted systems indicate that these vesicles have a well-defined diameter, which is in the range of 80 nm (5, 6). Although protein coats can adapt their size to form bigger vesicles for the packaging of large cargoes (7, 8), the converse has not been observed and transport vesicles smaller than 50 nm have rarely been reported. One exception are vesicles involved at early stages of autophagy, with a diameter in the range of 30 to 60 nm as estimated from morphological and hydrodynamic measurements (9, 10).

Surprisingly, a new class of transport vesicles has been recently identified through cellular investigations of tumor protein D54 (TPD54) (11). TPD54 is a small (206 aa, 22.2 kDa) protein that belongs to a family of four proteins: TPD52, TPD53 (or TPD52L1), TPD54 (or TPD52L2), and TPD55 (or TPD52L3) (12). These proteins are ubiquitously expressed in cells except TPD55, which is specific to the testis. Light microscopy imaging indicates that TPD54 associates with various membrane-bound compartments, mostly GA and endosomal structures (11). In addition, a large fraction of TPD54 is found in the cytosol but this localization is deceptive. Fluorescence recovery after photo bleaching (FRAP) experiments suggests that the cytosolic fraction of TPD54 corresponds to very small structures (≈32 nm), which could be resolved by super resolution microscopy (11). When TPD54 is redirected to the mitochondria by a knocksideway-based approach, it causes the accumulation of numerous small-sized vesicles (diameter ≈ 30 nm) at the mitochondria surface. Several lines of evidence suggest that these vesicles are involved in membrane traffic. First, deletion of TPD54 causes a severe Golgi dispersal phenotype as well as a delay in the secretion of a model cargo (E-cadherin). Second, TPD54 vesicles contain many Rab proteins, which are small G proteins involved in vesicular traffic, as well as Q-SNARE proteins, which promote vesicle fusion (11).

Here, we show that TPD54 recognizes highly curved membranes through the folding of adjacent amphipathic helices (AHs) including an amphipathic lipid packing sensor (ALPS) motif. ALPS are amphipathic sequences of 18 to 40 aa motifs that are characterized by the abundance of small polar residues (Gly, Ser, and Thr), by the rarity of charged residues and by the presence of regularly spaced bulky hydrophobic residues (13–17). ALPS motifs are intrinsically unstructured

* For correspondence: Bruno Antonny, antonny@ipmc.cnrs.fr.

but fold as AHs at the surface of highly curved membranes displaying lipid packing defects (15, 18–21). ALPS motifs are present in several proteins that transiently interact with highly curved membranes (22). These include the COPI coat regulators ArfGAP1 and Gcs1 (17, 23–26) and vesicle-tethering factors such as the golgin GMAP-210 (15, 16, 27, 28), the HOPS complex (29, 30) and synapsin (31). In addition, functional ALPS motifs are present in the sterol transfer protein Osh4 (32, 33), the autophagy protein ATG14L (34–36), the Golgi-associated PI-4 kinase PI4KIIIß (37) and some members of the nuclear pore complex (15, 38).

We show that TPD54 shows a sharp preference for highly curved and unsaturated lipid membranes *in vitro* and, as such, resembles previously characterized ALPS-containing proteins. In cells, mutating the ALPS motif of TPD54 abolished its association with disparate membranes. However, differences in localization between TPD54 and the golgin GMAP-210, which also captures small transport vesicles through an ALPS motif, suggest the involvement of additional interactions for the selection of specific small transport vesicles. In line with this hypothesis, binding of TPD54 to small liposomes is accompanied by a large structural change that applies not only to the ALPS motif but also to the full region downstream of the coiled-coil region.

Results

Bioinformatic analysis of TPD54

Figure 1 shows the domain organization of human TPD54 (206 aa) as deduced from several bioinformatic tools and previous experiments (11). Algorithms for the presence of intrinsically disordered regions suggest that the protein is roughly divided in four parts with different propensity to be folded (Fig. 1*A*). The first and last quarters of the protein (≈1–40 and 180–206) are predicted to be unstructured. The second quarter (≈40–100) shows a high probability to be folded. The third quarter (≈100–180) is ill-defined, being at the border between order and disorder. TPD54 also contains a predicted coiled-coil region, which spans from residue 38 to 82 (Fig. 1*B*) and which has been shown to contribute to homotypic and heterotypic associations between TPD protein members (39). The recently published machine learning method AlphaFold (40) (https://alphafold.ebi.ac.uk/) overall agrees with this architecture, predicting with high confidence (>0.9) an α-helix between aa E43 and R79 corresponding to the coiled-coil, whereas other regions are predicted as either random coils (M1-T42; V178-F206) or α-helical (T85-V102; S104-Q122; D124-R159; A162-K177) but with low or medium confidence (Fig. 1*C*).

We previously used the bioinformatic tool HELIQUEST (https://heliquest.ipmc.cnrs.fr/) (41) to detect the presence of ALPS motifs in the full human and yeast proteomes and identified TPD54 as one of the ≈ 200 human proteins containing an ALPS motif (15). The ALPS motif of TPD54 spans S141-M158. By rescanning the full TPD54 sequence with HELIQUEST, we observed that three other regions, two upstream and one downstream of the ALPS motif, also display an amphipathic helical sequence (Fig. 1*D*). They are referred to as AH1 (L83-V100), AH2 (Q101-V120), and AH4 (T163-G180), with AH3 corresponding to the ALPS motif. They all contain

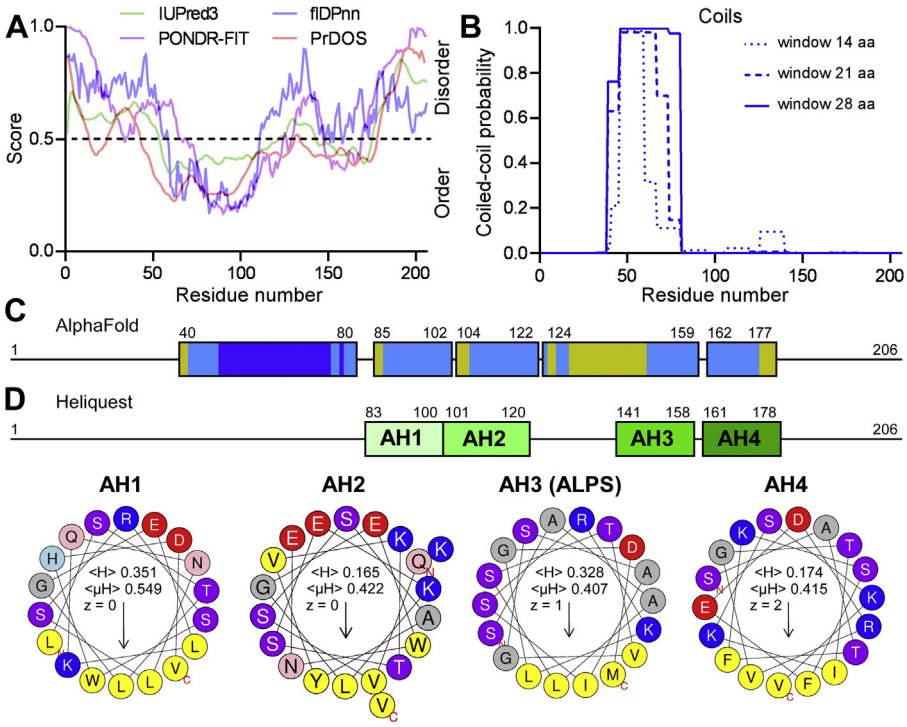

Figure 1. Bioinformatic analysis of TPD54. *A*, analysis of the TPD54 sequence using the indicated webtools for intrinsically disordered regions. *B*, coiled-coil prediction with *Coils*. *C*, helical structures as predicted by AlphaFold. The *color code* shows the degree of confidence: *high*, *dark blue*; *medium*, *light blue*; *low*, *yellow*. *D*, helical projections of the indicated sequences of TPD54 using HELIQUEST. The analysis suggests the presence of four amphipathic helices. *Color code*: *yellow*, hydrophobic residues; *blue*, basic; *red*, acidic; *purple*, Ser and Thr; *gray*, Ala and Gly; *pink*, Gln and Asn.

Gly residues, which should make them malleable for switching from a random coil to an α-helix in the presence of a proper membrane template. AH1, AH2, and AH4 are rich in both positively and negatively charged residues in contrast to ALPS motifs, which have a maximum of four charged (Asp, Glu, Lys, and Arg) residues (15, 17). Of note, AH1-AH2 as well as AH3-AH4 are not in register, which means that if they were forming a single continuous α-helix, their respective hydrophobic faces would point toward opposite directions.

Overall, the predicted domain organization of TPD54 with both a coiled-coil region and amphipathic motifs bears resemblance to the N-terminal region of the golgin GMAP-210, a very long coiled-coil protein. GMAP-210 acts as a tethering string, capturing small transport vesicles through its N-ter ALPS motif (16, 27, 42).

TPD54 binds to simple phospholipid vesicles in a curvature-dependent manner

We purified recombinant human TPD54 from a glutathione-*S*-transferase (GST) fusion form by a three-step protocol: (i) glutathione-bead binding step; (ii) thrombin cleavage of the linker between GST and TPD54; (iii) size-exclusion chromatography. To determine if TPD54 can directly interact with lipid membranes, we incubated full-length TPD54 with liposomes and recovered the liposome-bound fraction by flotation after centrifugation on sucrose cushions. Figure 2*A* shows the result of an experiment with three preparations of liposomes: phosphatidylcholine (PC)(18:1/18:1) (dioleoyl-phosphatidylcholine) obtained extrusion through 200 nm polycarbonate filters; PC(18:1/18:1) obtained by sonication; and PC(4ME 16:0/4ME 16:0) (diphytanoyl-PC) obtained extrusion through 200 nm polycarbonate filters. Diphytanoyl-lipids, which are not present in eukaryotic cells, form lipid membranes that are very permissive to the binding of AHs owing to the branched nature of their acyl chains, which favors hydrophobic insertions (43). TPD54 bound weakly to 200 nm PC(18:1/18:1) liposomes but strongly to sonicated PC(18:1/18:1) liposomes and to 200 nm PC(4ME 16:0/4ME 16:0) liposomes. Thus, TPD54 is able to interact directly with simple membranes (*i.e.*, PC) and binding is very

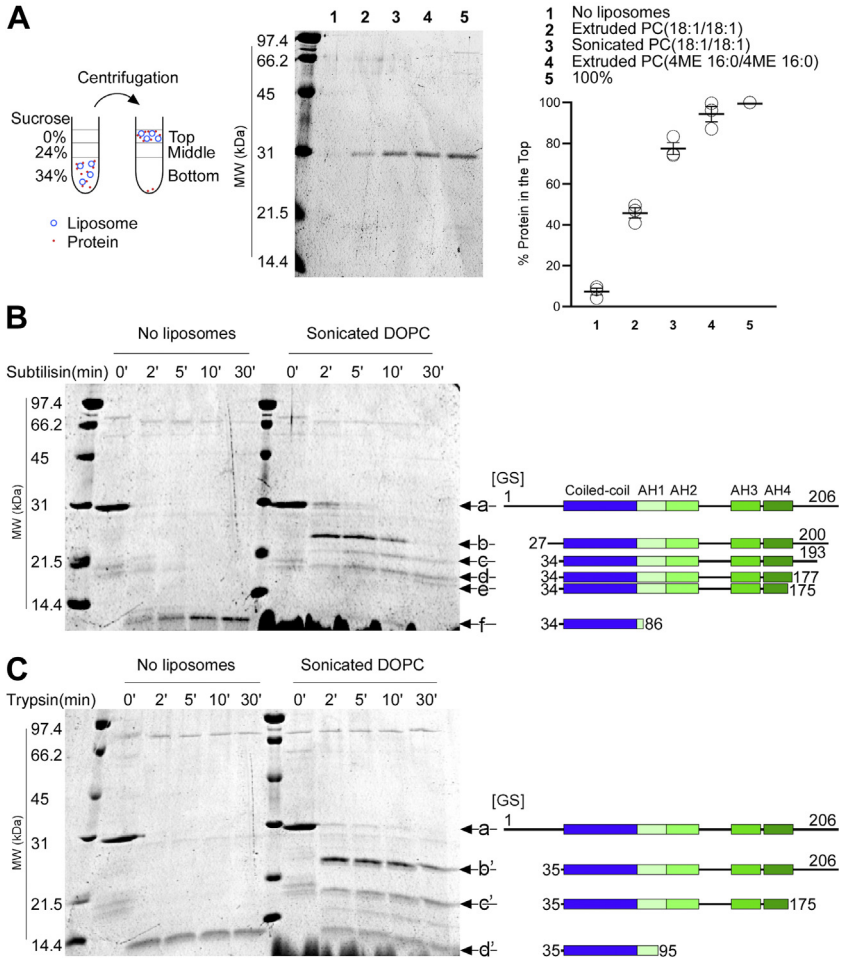

Figure 2. Limited proteolysis indicates that binding of TPD54 to small liposomes occurs through a large conformational change. *A*, flotation experiments of TPD54 with liposomes. After incubation of purified TPD54 with liposomes, the liposomes were recovered by flotation on sucrose cushions and analyzed by SDS-PAGE using Sypro-Orange staining. The gel shows the top (lipid) fraction. *Lane 5* is the amount of TPD54 added to each centrifugation tube. The graph on the *right* quantifies the gel bands from three independent experiments (*open circles*). The bars show the mean ± SEM. *B* and *C*, limited proteolysis of TPD54 with trypsin or subtilisin in the presence or in the absence of sonicated DOPC liposomes. Gels were stained with Sypro-*Orange*. The sequence of the various fragments was determined by mass spectrometry (see Tables S1 and S2).

sensitive to both membrane curvature and lipid acyl chain composition.

Large structural changes accompany the binding of TPD54 to membranes

To determine if structural changes accompany the binding of TPD54 to membranes, we conducted limited proteolysis experiments. For this aim, we incubated TPD54 with trypsin or subtilisin and analyzed the resulting fragments over time by SDS-PAGE and mass spectrometry (MS). Trypsin cleaves peptide bonds downstream of accessible Lys or Arg residues, whereas subtilisin cleaves accessible peptide bonds with poor sequence specificity. We noticed that TPD54 showed anomalous migration on SDS-PAGE with an apparent molecular weight (MW) close to 30 kDa, much higher than the calculated MW (22,368.32 Da), which included the N-terminal sequence "GS" arising from the linker between TPD54 and GST after cleavage with thrombin (Fig. 2*B*). This anomalous migration was systematic for all fragments analyzed and might be related to weaker SDS binding due to some intrinsic features of the TPD54 sequence (44). By MS, we observed that purified TPD54 had a mass of 22,367.245 Da, which corresponds to approximately a -1 Da shift *versus* the calculated mass (22,368.32 Da) (Tables S1 and S2).

In the absence of liposomes, trypsin and subtilisin rapidly digested TPD54, leading to the apparition of a single protease-resistant band with an apparent size below the lowest MW marker (14 kDa; Fig. 2*B*). MS identified this band as aa 34 to 86 and aa 35 to 95 in the case of subtilisin and trypsin digestion, respectively (Tables S1 and S2). In agreement with the bioinformatic analysis (Fig. 1), this result suggests that only a small part of TPD54, which corresponds to the predicted coiled-coil region, is intrinsically folded, whereas the remaining regions display no stable structure.

Incubation of TPD54 with sonicated liposomes caused an important protection of TPD54 from protease degradation. For both subtilisin and trypsin, a fragment with an apparent MW ≈ 24 kDa rapidly accumulated at t = 2 to 5 min before subsequent digestion into smaller fragments of apparent MW of 23 to 19 kDa (Fig. 2*B*). Analysis by MS suggested that the first 33 or 34 aa, which are upstream of the predicted coiled-coil, were rapidly degraded. In contrast, the region downstream of the coiled-coil region appeared essentially intact at early time points (t = 2–5 min) and became slowly digested into smaller fragments. In the case of subtilisin, MS analysis suggested gradual digestion of the C terminus according to the series aa 206 > 200 > 193 > 177 > 175, that is, up to the fourth predicted AH) (Fig. 2*B*). Digestion with trypsin occurred *via* less intermediates but also led to the apparition of a fragment (35–175), which was observed only in the presence of sonicated liposomes and which encompassed both the coiled-coil region and the four predicted AHs. As observed for full-length TPD54, most fragments showed a ≈−1 Da shift in mass as compared to the calculated mass (Tables S1 and S2).

Altogether, the results of the limited proteolysis experiments suggest that the recognition of small vesicles by TPD54 leads to major changes in the protein structure and/or accessibility to solvent, which applies to the full region downstream of the predicted coiled-coil region.

TPD54 binding to small liposomes is accompanied by α-helical folding

Given the fact that the region that becomes protected from proteolysis in the presence of small liposomes contains the four predicted AHs (AH1-AH4), we performed CD experiments to determine if changes in the secondary structure accompanies TPD54 adsorption to small liposomes. In solution, the CD spectrum of TPD54 featured two minima at 208 and 222 nm, which are characteristic of α-helical structures. Upon addition of sonicated PC(18:1/18:1) liposomes, these two negative peaks further increased, suggesting additional folding of α-helical regions (Fig. 3*A*). Fitting the CD spectra using the web tool CAPITO (https://data.nmr.uni-jena.de/capito/index.php) (45) suggests that the content in α-helix increased from 30% in solution to 60% in the presence of sonicated PC(18:1/18:1) liposomes. Considering that the coiled-coil region of TPD54 is 45 aa whereas each predicted AH (AH1 to AH4) is about 18 aa in length, this twofold increase in helicity suggests the folding of the equivalent of two to three of these helices.

Tryptophan fluorescence reveals conformational changes in the 85 to 140 region

The TPD54 region downstream of the predicted coiled-coil contains two tryptophan residues (W97 and W116), whereas no other tryptophan is present in the TPD54 sequence (Fig. 1*D*). Because tryptophan fluorescence is very sensitive to environmental changes and because this region becomes fully protected from protease degradation in the presence of sonicated PC(18:1/18:1) liposomes, we compared the intrinsic fluorescence of TPD54 in the absence and in the presence of such liposomes. As shown in Figure 3*B*, binding of TPD54 to sonicated PC(18:1/18:1) liposomes promoted a large tryptophan fluorescence increase, which was accompanied by a blue shift. This observation further strengthens the hypothesis that binding of TPD54 to curved membranes leads to a large reorganization of the protein structure, including the region encompassing the two tryptophan groups.

According to HELIQUEST (41), W97 and W116 belong to the hydrophobic faces of the putative AHs, AH1 and AH2, respectively (Fig. 1*D*). To determine whether tryptophan W97 and/or W116 become close to the membrane interfacial region upon TPD54 binding to small liposomes, we conducted FRET experiments. We used PC(18:1/18:1) liposomes doped with 5 mol% of the fluorescent lipid diphenylhexatriene PC (DPH-PC). The excitation spectrum of DPH-PC overlaps with the emission spectrum of tryptophan, thereby leading to a FRET signal when tryptophan groups partition in lipid membranes (46, 47). Stepwise additions of TPD54 to sonicated DPH-PC-containing liposomes induced a FRET signal, whereas no increase was observed with extruded liposomes (Fig. 3*C*). These results suggest that W97 and/or W116 become close enough to the membrane interface (FRET distance is typically in the nanometer range) when TPD54 adsorbs onto highly curved PC liposomes but do not interact with flat surfaces.

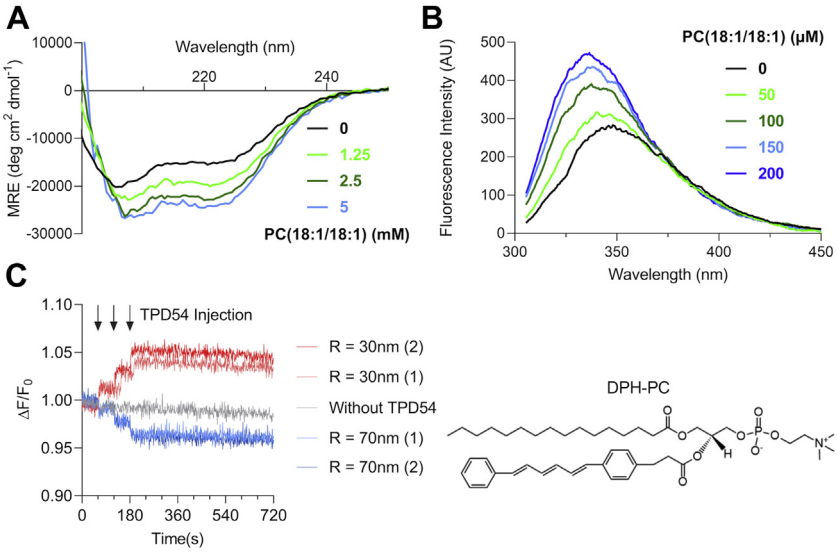

Figure 3. Binding of TPD54 to small liposomes promotes an increase in α-helicity and a change in tryptophan exposure. *A*, CD spectra of TPD54 (4 μM) in the absence or in the presence of increasing concentration of sonicated PC(18:1/18,1) liposomes. *B*, fluorescence emission spectra of TPD54 in the presence of increasing concentrations of sonicated PC(18:1/18,1) liposomes. *C*, FRET assay between TPD54 tryptophan residues and DPH-PC. The fluorescence cuvette initially contained PC liposomes (200 μM total lipids; PC(18:1/18:1) 95 mol%, DPH-PC 5 mol%) in HKM buffer. Fluorescence at 460 nm upon excitation at 280 nm was continuously recorded upon the sequential addition of TPD54 (3 × 250 nM; *vertical arrows*). The *red* and *blue traces* show two independent experiments performed with sonicated liposomes (radius 30 nm) and extruded (200 nm) liposomes (radius 70 nm), respectively. The *gray trace* shows the evolution of the fluorescence signal without any protein addition. Each protein addition diluted the sample by 1.3 %. This dilution factor explains the drop observed for the experiments performed in the presence of extruded liposomes. The structure of DPH-PC is shown on the right. DPH-PC, diphenylhexatriene PC; PC, phosphatidylcholine.

Membrane proximity analysis using nitrobenzoxadiazole-cysteine scanning mutageneis

To map the TPD54 membrane-interacting regions in a more extensive manner, we prepared various cysteine mutants, which we labeled with the membrane-sensitive fluorescent probe nitrobenzoxadiazole (NBD). We selected seven positions, which flank the five predicted structural elements in the following order: A37C - coiled-coil - G82C - AH1 - Q101C - AH2 - S123C - G137C - AH3 - S161C - AH4 - G185C (Fig. 4). In flotation experiments, all mutants showed stronger binding to sonicated PC(18:1/18:1) liposomes than to extruded ones (200 nm) (Fig. S1). However, we observed strong differences between the NBD-labeled forms when we recorded their fluorescence in the presence or absence of liposomes. When NBD flanked the predicted AHs AH1, AH2, and AH3 (mutants G82C-NBD, Q101C-NBD, S123C-NBD, G137C-NBD ,and S161C-NBD), we observed a large (twofold to threefold) increase in NBD fluorescence upon the addition of sonicated PC(18:1/18:1) liposomes or extruded (200 nm) PC(4ME 16:0/4ME 16:0) liposomes (Fig. 4*A*, *magenta* and *blue spectra*, respectively). As expected, no fluorescence change was observed in the presence of large PC(18:1/18:1) liposomes (Fig. 4*A*, *green spectra*). In contrast, TPD54 A37C-NBD, in which the fluorescent probe is upstream of the predicted coiled-coil, showed no fluorescence change, whereas TPD54 G185C-NBD, in which the fluorescent probe is downstream of the fourth predicted AH (AH4) showed a modest (x 1.2–1.3) fluorescence increase in the presence of either sonicated PC(18:1/18:1) liposomes or extruded (200 nm) PC(4ME 16:0/4ME 16:0) liposomes. Overall, the results of the NBD cysteine scanning mutagenesis, which are summarized in Figure 4*B*, were in good agreement with the limited proteolysis experiments and suggested that the three predicted AHs AH1, AH2, and AH3 become close to the membrane interface when TPD54 adsorbs to membranes.

TPD54 binds cellular structures through AH2 and AH3 (ALPS)

Next, we tested the contribution of AH1, AH2, AH3 (ALPS), and AH4 to the subcellular distribution of TPD54. For this aim, we expressed full-length TPD54, which was N-terminally fused with GFP, in RPE1 cells and analyzed the effects of mutations that should decrease the interaction of these putative AHs with the lipid membrane. We selected four mutations L93D (AH1), L113D (AH2), I151D (AH3), and V171D (AH4), which introduce a negative charge in the hydrophobic face of the putative helices.

At moderate expression level, WT GFP-TPD54 showed a composite distribution pattern. In agreement with a previous study (11), GFP-TPD54 distributed between a cytosolic pool, a perinuclear fraction, and some rounded structures scattered in the cytoplasm (Fig. 5*A*). The perinuclear fraction corresponded to the GA, showing apposed localization with Golgi markers (Fig. S2). Mutating the first (L93D) or the fourth (V171D) predicted AH caused no significant change in the distribution of the protein, whereas mutating the second (L113D) predicted AH significantly reduced the Golgi pool of TPD54 (Fig. 5, *A* and *B*). Strikingly, when we introduced the disruptive I151D mutation in AH3, that is the ALPS motif, GFP-TPD54 no longer decorated intracellular structures and appeared essentially cytoplasmic (Fig. 5, *A* and *B*).

Larocque *et al.* showed that the apparent cytoplasmic pool of TPD54 as seen by conventional microscopy is misleading:

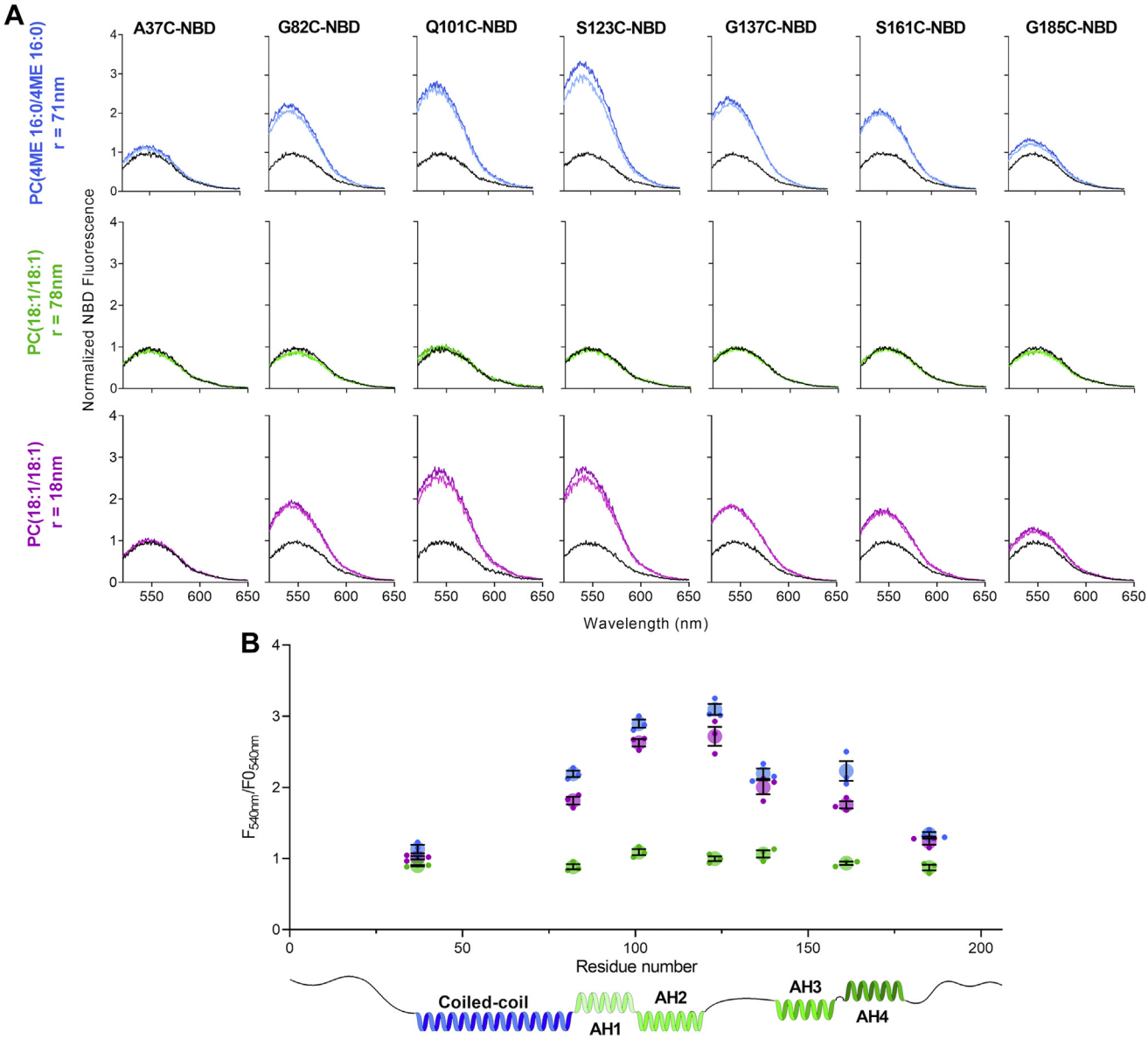

Figure 4. Mapping the TPD54 membrane interaction by NBD fluorescence. *A*, emission fluorescence spectra of NBD-labeled TPD54 (100 nM) at the indicated position in buffer (*black curves*) or in the presence of 50 μM (*light color curves*) or 100 μM PC liposomes (*dark color curves*). The liposomes were extruded (200 nm) PC(4ME 16:0/4ME 16:0) (*blue curves*), extruded (200 nm) PC(18:1/18,1) (*green curves*) or sonicated PC(18:1/18,1) (*magenta curves*). *B*, quantification of the change in NBD fluorescence at 540 nm as a function of the position of the labeled cysteine from three independent experiments similar to that shown in A. The small symbols show the results of each experiment. The large symbols and associated error bars show mean ± SEM. ; NBD, nitrobenzoxadiazole; PC, phosphatidylcholine.

FRAP measurements and flickering analysis of the GFP-TPD54 signal in the cytoplasm suggested association to vesicular structures (11). We performed FRAP measurements of some GFP-TPD54 constructs in selected subcellular regions, including the cytoplasm, the rounded structures, and the GA (Fig. 5*C*). WT GFP-TPD54 and GFP-TPD54[V171D] recovered from these structures as well as from the cytoplasm with comparable rate constants, which were in the range of 0.2 to 0.37 s^{-1}. The recovery curves, which could be well resolved, were ca 4 to 6 times slower than what was observed with pure GFP (1.25 s^{-1}), suggesting that GFP-TPD54 was rarely soluble, even when present in the cytoplasmic fraction. Strikingly, when GFP-TPD54 was mutated in its ALPS motif (I151D), which led to its complete redistribution in the cytoplasm, its recovery rate was very fast (1 s^{-1}), similar to that of isolated GFP (1.25 s^{-1}) and much faster than WT GFP-TPD54, whether in the cytoplasm (0.37 s^{-1}) or on visible structures (Fig. 5*C*). These static and dynamics observations indicate that the ALPS motif of GFP-TPD-54 makes a major contribution to the association of the protein to various subcellular structures, including cytoplasmic structures, which were previously identified as nanovesicles.

TPD54 lipid-binding properties resemble that of other ALPS-containing proteins

Whereas the results of the limited proteolysis experiments and of NBD/Cys scanning mutagenesis suggest major rearrangements of all regions encompassing AH1 to AH4 (Figs. 2

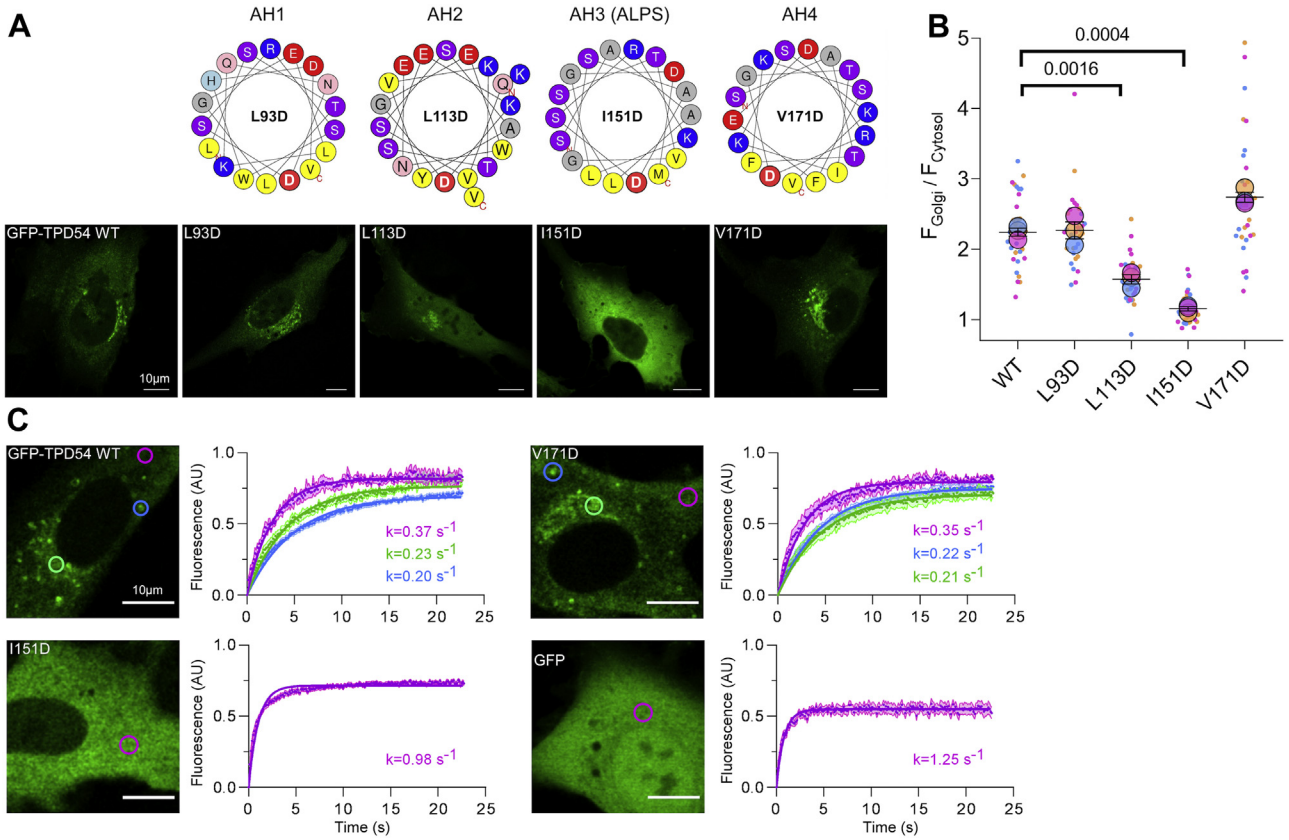

Figure 5. The ALPS motif contributes to TPD54 subcellular localization. *A*, representative confocal images of RPE1 cells expressing WT GFP-TPD54 or mutants harboring a negative charge in one of the four putative amphipathic helices. Mutating the ALPS motif makes TPD54 cytosolic. *B*, quantification of experiments similar to that shown in (*A*) using Superplot representation. Each *dot* represents one cell that is *color*-coded according to the biological replicate it comes from. The *large circles* represent the mean of each replicate. The three means were then used to calculate the average ± SEM (*black bars*) (65). Thirty cells from three independent experiments were analyzed for each mutant. The numbers on the plot show the *p* value for sameness. *C*, dynamics of GFP-TPD54 or of mutants in AH3 or in AH4 as assessed by FRAP analysis in various subcellular regions. Pure GFP was used as a control cytosolic protein. The recovery curves were fitted with a monoexponential equation ($F = F_0(1 - e^{-kt})$). Data show are mean ± SEM from 10 to 20 FRAP assays and from two cell transfections. The scale bar represents 10 µm. ALPS, amphipathic lipid packing sensor; FRAP, fluorescence recovery after photo bleaching.

and 4), the cellular experiments highlight a prominent role of AH2 and AH3 (ALPS) in TPD54 localization. To directly assess the role of these regions in the membrane-binding properties of TPD54, we performed liposome-binding experiments with TPD54 mutants. For this aim we combined a disruptive mutation in the AH of interest (L113D for AH2, I151D for AH3) with the NBD-labeling of neighboring cysteine (Q101C-NBD for AH2 and S161C-NBD for AH3) (Fig. 6, *A* and *B*). In addition, we prepared a mutant harboring both the reporter mutation S161C-NBD and a disruptive mutation in AH4 (V171D).

Titration experiments with increasing concentration of sonicated PC(18:1/18:1) liposomes showed that TPD54 [Q101C-NBD, L113D] had a threefold decrease in affinity for liposomes as compared to TPD54[Q101C-NBD] (Fig. 6*A*), whereas TPD54[I151D, S161C-NBD] had a 10-fold decrease in affinity for liposomes as compared to TPD54[S161C-NBD (Fig. 6*B*). In contrast, the liposome-binding properties of TPD54[S161C-NBD] and of TPD54[S161C-NBD, V171D] were similar. Moreover, a mutant with disruptive mutations in both AH3 and AH4 (TPD54[I151D, S161C-NBD, V171D]) showed a similar dose–response curve as the AH3 mutant. These experiments suggested that AH2 and AH3 are directly involved in TPD54 binding to curved membranes.

Next, we performed titration experiments using liposomes made of either PC(18:1/18:1), PC(16:0/18:1) (1-palmitoyl 2-oleoyl phosphatidylcholine), or PC(14:0/14:0) (dimyristoyl phosphatidylcholine). We observed marginal binding of TPD54[S161C-NBD] to PC(16:0/18:1) or PC(14:0/14:0) liposomes made by extrusion ($K_d \approx 2$ mM; radius ≈ 70 and 90 nm, respectively) (Fig. 6*C*) but more significant binding to extruded PC(18:1/18:1) liposomes ($K_d \approx 300$ µM; radius ≈ 65 nm). With sonicated PC(18:1/18:1) or PC(16:0/18:1) liposomes (radius = 30 and 25 nm, respectively), binding was much stronger ($K_d \approx$ 20 and 25 µM; respectively), whereas barely any binding occurred with sonicated (radius 22 nm) PC(14:0/14:0) liposomes ($K_d \approx 700$ µM) (Fig. 6*C*). Overall, the affinity of TPD54 [S161C-NBD] for PC liposomes varied by two orders of magnitude (from K_d = 20 µM to 2 mM) depending on PC unsaturation and liposome size (Fig. 6*C*). This hypersensitivity to both membrane curvature and lipid unsaturation is a biochemical feature of ALPS motifs.

Finally, we compared the liposome-binding properties of TPD54 with other ALPS-containing constructs, namely the N-terminal region of GMAP-210 and the first ALPS motif of ArfGAP1 (Fig. S3). With PC(16:0/18:1) liposomes, GMAP-210 [M1C-NBD, 1–189], ArfGAP1[192–257, A236C-NBD], and

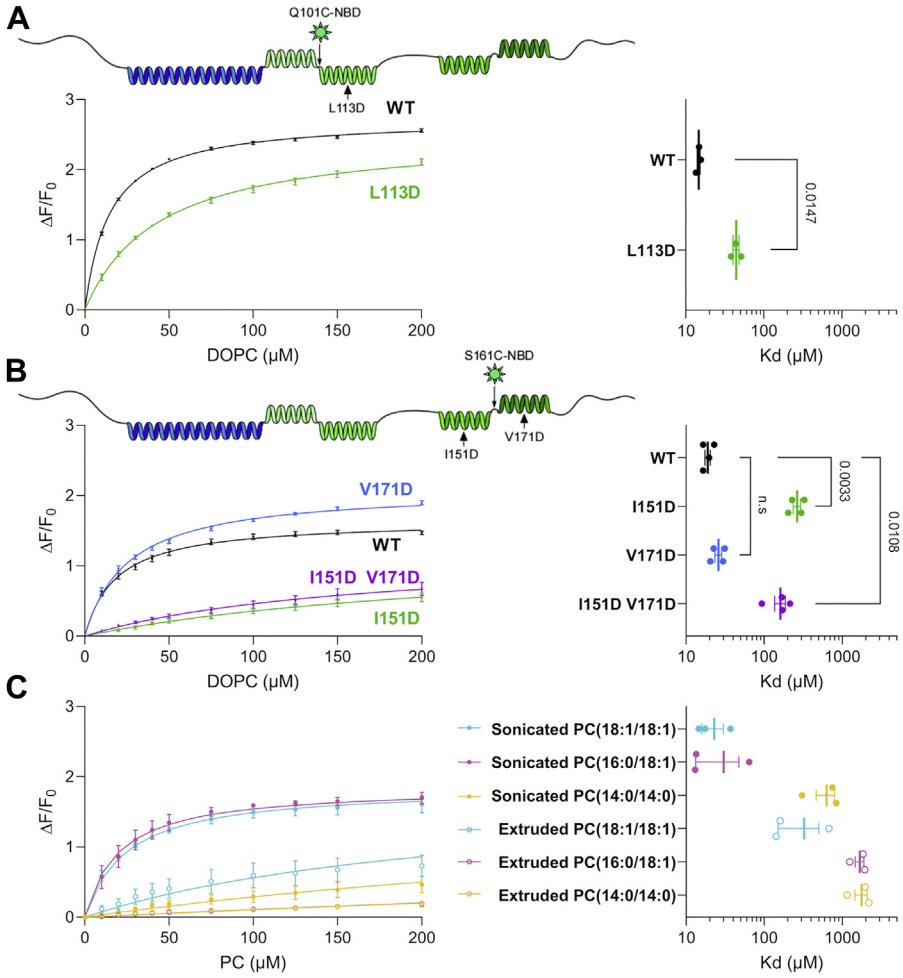

Figure 6. TPD54 interacts with small liposomes through AH2 and AH3. *A* and *B*, impact of disruptive mutations in AH2 (L113D), AH3 (I151D), or AH4 (V171D) on TPD54 binding to sonicated PC(18:0:18:1) liposomes. The mutations were tested on TPD54 carrying the membrane reporter NBD either at position Q101C (*A*) or S161C (*B*). In all cases, the fluorescence at 530 nm of the protein (100 nM) was used to build liposome-binding curves, which were fitted with hyperbolic functions $\left(\Delta F = \Delta F_{max}\left(\frac{[L]}{K_d+[L]}\right)\right)$ to determine apparent K_d. Data show mean ± SEM from three (*A*) or four (*B*) independent titration curves conducted with two preparations of liposomes. *C*, dual effect of membrane curvature and lipid unsaturation on the binding of TPD54-S161C-NBD to PC liposomes. Liposomes were made of PC(18:1/18:1), PC(16:0/18:1), or PC(14:0/14:0) and were prepared by extrusion (200 nm; *open symbols*) or by sonication (*filled symbols*). The titration curves were determined from the fluorescence of TPD54-S161C-NBD (100 nM) at 530 nm. The *right plot* shows the apparent K_d as deduced from hyperbolic fits. Data show mean ± SEM from three independent experiments conducted with different preparations of liposomes. AH, amphipathic helix; NBD, nitrobenzoxadiazole; PC, phosphatidylcholine.

TPD54[S161C-NBD] showed binding to small liposomes (R = 39 nm) but not to larger ones (R in the 82–105 nm range). We also added 30% of the negatively charged lipid PS(16:0/18:1), which strongly favors the membrane binding of positively charged AHs but has minor effects on ALPS motifs (48). PS(16:0/18:1) had a slight positive effect on TPD54, the binding of which could be observed even with extruded liposomes.

Altogether, the liposome-binding experiments indicate that TPD54 contains two main membrane-interacting AHs, AH2 and AH3. The latter, which corresponds to an ALPS motif, makes the highest contribution to liposome binding, thereby accounting for the preference of TPD54 for highly curved and unsaturated membranes.

TPD54 and GMAP-210 do not recognize the same vesicular structures

Several lines of evidence suggest that the golgin GMAP-210 recognizes endogenous vesicles through its N-terminal ALPS motif. Notably, correlative light-electron microscopy showed that when GMAP-210 lacked its ALPS motif, it failed to restore the Golgi ultrastructure of cells in which the expression of endogenous GMAP-210 was silenced, whereas full-length GMAP-210 restored the balance between vesicles and cisternae (28). Given the involvement of an ALPS motif in the recognition of small transport vesicles by TPD54, we wondered whether GMAP-210 and TPD54 might recognize a common set of transport vesicles, which should lead to some overlap in their respective localization.

We analyzed the localization of endogenous GMAP-210 and TPD54 or of overexpressed protein constructs. Given the small size of transport vesicles and the complex organization of the GA, we conducted this analysis using stimulated emission-depletion (STED) microscopy in addition to conventional confocal microscopy. When we compared STED images of endogenous TPD54 and of endogenous GMAP-210 using specific antibodies, the signals from the two proteins did not

overlap, although they both stained the Golgi region (Fig. 7). In addition, the signal of slightly overexpressed Halo-tag-TPD54 did not coincide with that of endogenous GMAP-210. Similarly, the signal from a Halo-tag construct that consisted in the N-terminal ALPS motif of GMAP-210 fused to an artificial coiled-coil (16) was clearly separated from the signal of endogenous TPD-54. We concluded that GMAP-210 and TPD54 do not bind the same cellular structures despite both harboring functional ALPS motifs.

To further analyze the difference in localization of GMAP-210 and TPD54 and the involvement of their amphipathic motifs, we prepared GMAP-210/TPD54 chimera in which we replaced the ALPS motif of GMAP-210 with either the ALPS motif (AH3; chimera 1) of TPD54 or a sequence encompassing both AH2 and AH3 (chimera 2) (Fig. 8*A*). These chimera were essentially cytoplasmic in marked contrast with another coiled-coil-based chimera (chimera 3) containing the ALPS motif of GMAP-210 (16, 49), which clearly stained the GA (Fig. 8*B*). This result suggests that AH2 and AH3 of TPD54, although important for membrane binding, are not sufficient when put in a different protein context. Of note, the ALPS motif of TPD54 (18 aa) is twice as short as that of GMAP-210 (38 aa), and previous experiments showed that the entire sequence of the ALPS motif of GMAP-210 contributed to membrane binding (16).

Discussion

The discovery that the protein TPD54 captures intracellular vesicles that are smaller than conventional transport vesicles (≈30 *versus* 60 nm in diameter) came as a surprise since it was generally assumed that the repertoire of transport vesicles in cells was complete (11). The present study, which combines an in-depth biochemical analysis of TPD54 with cellular

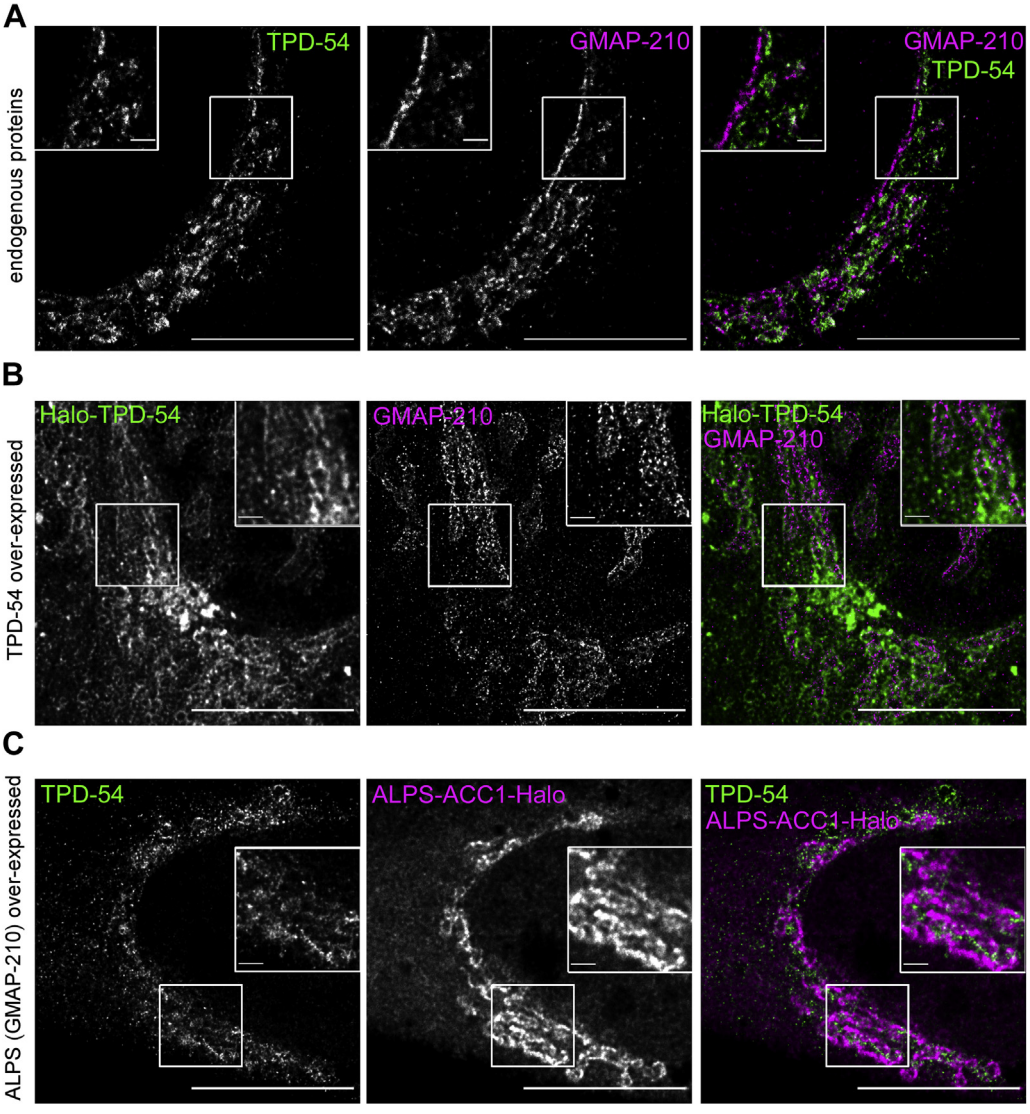

Figure 7. TPD54 and the golgin GMAP-210 bind different cellular structures. STED Imaging of TPD-54 as compared to GMAP-210 in RPE1 cells. *A*, endogenous TPD-54 *versus* endogenous GMAP-210. *B*, overexpressed Halo-TPD-54 *versus* endogenous GMAP-210. *C*, endogenous TPD-54 *versus* a construct made of the ALPS motif of GMAP-210, an artificial coiled-coil, and a Halo-tag (GMAP-210-ACC1-Halo). The scale bar represents 10 μm (main panels), 1 μm (insets). STED, stimulated emission-depletion.

observations, gives a molecular basis for the capture of small vesicles by TPD54.

CD spectroscopy and limited proteolysis experiments indicate that isolated TDP54 is largely disordered except for its predicted coiled-coil region. Upon binding to small liposomes, TPD54 undergoes a huge structural change, which affects the entire region downstream of the coiled-coil, that is from aa 85 up to amino-acid 200, and which correlates with a gain in α-helicity. In contrast, the region upstream of the coiled-coil remains unfolded and remote from the membrane. Among the regions that become folded upon membrane association, AH2 and AH3 of TPD54, which encompasses aa 101 to 120 and aa 141 to 158, respectively, make a key contribution to membrane interaction. A single negative charge in the hydrophobic face of AH2 or AH3 lowered the avidity of purified TPD54 for small liposomes by 3-fold or 10-fold, respectively, and reduced (AH2) or even abolished (AH3) the membrane partitioning of the protein in cells.

TPD54 binds to lipid membranes in a sharp curvature-dependent and lipid unsaturation–dependent manner. We did not detect binding of TPD54 on liposomes with a diameter $>$ 60 nm except when using the nonphysiological lipid PC(4ME-16:0/4ME-16:0), which creates large lipid-packing defects even in flat membranes (43). For liposomes made of PC(16:0/18:1), which is the most abundant PC species in cellular membranes, TPD54 shows binding only when the liposome diameter is below 60 nm. The hypersensitivity of TPD54 to membrane curvature and lipid unsaturation contrasts with its low sensitivity to liposome charge as binding was poorly dependent on the general anionic lipid phosphatidylserine (PS). Although we cannot exclude that TPD54 is sensitive to some specific lipids that were not tested here, the dual sensitivity of TPD54 to both membrane curvature and lipid unsaturation makes TPD54 similar to other ALPS motif–containing proteins as regard to membrane-binding properties (13, 14, 22).

Whether the ALPS motif of TPD54 has a curvature threshold different from other ALPS motifs, making it more adapted for the capture of nanovesicles with a diameter of 30 nm as compared to vesicles with a diameter of 60 to 80 nm, awaits further investigation. The assays used here are based on bulk measurements with liposomes prepared by sequential extrusion through polycarbonate filters or by sonication. As previously documented by electron microscopy and dynamic light scattering measurements (50, 51), these methods give liposomes that display polydispersity around an average size value. To further characterize the exact curvature preference of TDP54, other methods will be necessary. These include quantitative fluorescence microscopy to measure curvature-selective binding of protein on immobilized single liposomes (52, 53) or on tubes pulled from giant unilamellar vesicles (24, 54).

The facts that membrane-dependent restructuring of TPD54 is not restricted to its ALPS motif and that the subcellular localization of TPD54 differs from that of the golgin GMAP-210, which also recognizes transport vesicles through an ALPS motif, suggest that other determinants cooperate with the ALPS motif

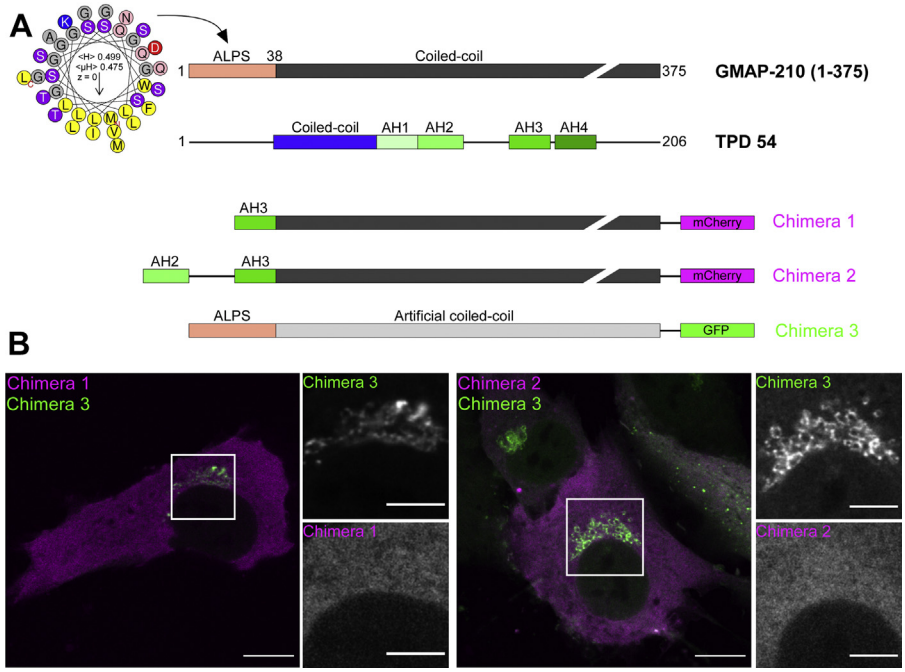

Figure 8. Subcellular localization of fusion constructs carrying the AH3 or AH2-AH3 region of TPD54 or the ALPS motif of GMAP-210. *A*, scheme of the constructs. Chimera 1, ALPS(TPD54)-GCC-mCherry, consists of the ALPS motif of TPD54 (aa 141–158), part of the coiled-coil region of GMAP (aa 39–375), and mCherry as a fluorescent reporter. Chimera 2, AH2-ALPS-(TPD54)-GCC-mCherry, consists of the AH2-AH3 region of TPD54 (aa 101–158), part of the coiled-coil region of GMAP (aa 39–375), and mCherry as a fluorescent reporter. Chimera 3, ALPS(GMAP-210)-ACC1-GFP, consists of the ALPS motif of GMAP-210 (aa 1–38), an artificial coiled-coil, and GFP as a fluorescent reporter. The use of the artificial coiled-coil prevents the formation of heterodimers with the construct containing the GMAP-210 coiled coil, hence facilitating their comparison (16, 49). *B*, comparison of the subcellular distribution of the chimera in RPE1 cells. The scale bar represents 10 μm (main panels), 5 μm (insets). AH, amphipathic helix; ALPS, amphipathic lipid packing sensor.

to make TPD54 and the golgin GMAP-210 specific to different populations of vesicles. In the case of GMAP-210, both the ALPS motif and the very first N-terminal residues are involved in the capture of different vesicles (55). For TPD54, a recent study based on the localization of various GFP constructs and on the effect of FKPB-TPD54 constructs on mitochondria aggregation suggests that region 83 to 126 and a set of basic residues (K154, R159, K175, and K177) are involved in intracellular nanovesicle recognition, although the underlying mechanism is not known (56). Our study approximately agrees with this mapping, showing the contribution of two membrane-interacting AHs with different chemistries in the recognition of small vesicles by TPD54. Interestingly, recent *in vivo* investigations suggest that minor changes in AH chemistry can lead to major effect *in vivo*, despite the fact some unrelated amphipathic sequences can substitute for each other (57). Therefore, the presence of AH2, AH3, and other determinants in TPD54 might provide a unique combinatory code to select a particular class of transport vesicles.

Determining how the various amphipathic regions of TPD54 cooperate to selectively capture intracellular nanovesicles through protein–protein and protein–membrane interactions will require numerous investigations because their disordered nature makes structural investigations difficult. α-Synuclein and CTP:phosphocholine cytidylyltransferase α provide nice examples of such efforts where extensive mutagenesis coupled to spectroscopic methods (*e.g.*, fluorescence and electron paramagnetic resonance) enable to establish the geometry of these amphitropic proteins at the membrane surface (58, 59). We considered unlikely that all four predicted AHs of TPD54 (from AH1 to AH4) directly contribute to lipid membrane interactions as this would require strong distortion in the regions separating them to allow their hydrophobic faces to point simultaneously toward the membrane. Nevertheless, the identification of two functional membrane-interacting AHs including an ALPS motif in TPD54 gives a first hint for the mechanism of selective capture of very small transport vesicles by this protein.

Experimental procedures

Bioinformatic analysis

We predicted the presence of intrinsically disordered regions in TPD54 using the following servers. PrDOS (https://prdos.hgc.jp/cgi-bin/top.cgi) predicts natively disordered regions from the amino acid sequence (60). PONDR-Fit (http://original.disprot.org/pondr-fit.php) combines the outputs of several individual disorder predictors (61). IUPred3 (https://iupred.elte.hu/) is based on an energy estimation method (62). flDPnn (http://biomine.cs.vcu.edu/servers/flDPnn/) predicts disorder using a neural network (63). We used the software coils (https://embnet.vital-it.ch/software/COILS_form.html) for the presence of coiled-coil regions (64) and AlphaFold (https://alphafold.ebi.ac.uk/) for the overall structure of TPD54 (40).

Molecular biology

The TPD54 sequence was amplified from HeLa cell RNA extracts by RT-PCR. The TPD54 sequence was subcloned into a pGEX-2T vector at the BamH1 and EcoR1 sites, that is, following the GST and the thrombin cleavage site. Mutations were introduced with the QuickChange Lightning kit (Agilent). The full sequence and the presence of the desired mutation were verified by automated sequencing.

Protein expression and purification

We expressed TPD54 as a GST fusion in *Escherichia coli* BL21. Bacteria were grown in LB supplemented with 100 μg/ml ampicillin at 37 °C. Protein expression was induced by the addition of 1 mM IPTG at absorbance = 0.8 for 1 h 30′ at 37 °C. Bacteria were lysed in a cell disruptor at 1600 psi in Tris 50 mM pH 7.4, NaCl 150 mM, and DTT 2 mM. After addition of 0.1 mg/ml DNAse and 5 mM $MgCl_2$, the soluble fraction was collected by centrifugation at 40,000 rpm for 30 min in a Ti45 rotor (Beckman). The fusion protein was purified from the soluble fraction using glutathione-Sepharose 4B beads at a vol/vol ratio of 4 ml beads for 100 ml supernatant. TPD54 was released from the beads by thrombin cleavage (12U/ml in the presence 50 μM $CaCl_2$) of the linker between GST and TPD54, which leaves the sequence "GS" at the N terminus of the protein. TPD54 was further purified by gel-filtration on a Sephadex S300 HR column in 20 mM Tris pH 7.4, 150 mM NaCl, 10% vol/vol glycerol, and 1 mM DTT. Aliquots were flash-frozen in liquid nitrogen and stored at −80 °C. Purification of ArfGAP1 ALPS1 motif (192–257, A236C-NBD) has been described elsewhere (17, 23). GMAP-210 (M1C-NBD, 1–189) was prepared from our previous construct GMAP-210 (M1C-NBD, 1–375) and purified and labeled with the same protocol (15).

Protein labeling with fluorescent probes

Cysteine mutants of TPD54 were labeled with NBD using a 10-fold excess of IANBD amide (N,N′-dimethyl-N-(iodoacetyl)-N'-(7-nitrobenz-2-oxa-1,3-diazol-4-yl)ethylenediamine) in 50 mM Tris pH 7.4, 150 mM NaCl. The time and temperature of labeling was optimized to limit the labeling of the sole endogenous cysteine (C74), which was found to have limited reactivity due to its intra coiled-coil localization. Excess probe was blocked with L-cysteine and removed by size-exclusion chromatography. The concentration of labeled protein was determined by absorbance at 500 nm.

Liposome preparation

Lipids were mixed as chloroform solutions and dried in a rotary evaporator. The lipid film was resuspended in HK buffer (50 mM Hepes pH 7.2, 120 mM K acetate), and the suspension was frozen and thawed five times to promote the formation of unilamellar liposomes followed by sequential extrusion through polycarbonate filters of decreasing pore size (200, 100, 50, and 30 nm). To further decrease the liposome size, the liposome suspension was sonicated using a probe sonicator. The average liposome size and polydispersity were determined by dynamic light scattering using a Cordouan Vasco Kin particle size analyzer. As small liposomes have tendency to fuse, they were used within the same day of preparation.

Liposome flotation assay

Liposomes (250 μM) and TPD54 (1 μM) were incubated for 5 min in 50 mM Hepes pH 7.2, 120 mM K acetate, 1 mM $MgCl_2$ (HKM buffer) at room temperature (RT) in a Beckman polycarbonate centrifuge tube. The mixture (75 μl) was mixed with HK buffer supplemented with 60% sucrose (100 μl) and then overlaid with an intermediate sucrose solution made of HK buffer with 24% sucrose (100 μl) and a layer (25 μl) of HKM buffer. After centrifugation at 100,000 rpm in a fixed-angle TLA100 rotor for 1 h, three fractions (bottom, medium, and top) of 175, 75, and 50 μl were collected and then analyzed by SDS-PAGE using Sypro-Orange staining.

Limited proteolysis

Proteins (2 μM) were mixed in HKM buffer with or without sonicated PC(18:1/18:1) liposomes at a protein/lipid mol:mol ratio of 1/1000 to get maximal membrane binding of TPD54. Trypsin or subtilisin (1 μg/ml) was added at time zero under agitation. At the indicated times, aliquots were withdrawn and the reaction was stopped by adding 0.5 μM PMSF. The reaction was analyzed by SDS-PAGE with Sypro-Orange staining and by MS.

MS analysis—μHPLC-Q-exactive plus

The sample was analyzed by liquid chromatography coupled to a mass spectrometer equipped with a heated electrospray ionization probe. HPLC was performed using a Dionex U3000 RSCL instrument. The injection volume was fixed at 5 μl (Ultimate 3000, Thermo Fisher Scientific). Protein analysis was performed on a 2.1 mm i.d. × 150 mm, 5 μm, Syncronis C18 column at a flow rate of 250 μl/min. The elution program was based on water (solvent A) and acetonitrile (solvent B) both containing 0.1% formic acid (v/v): 0 min 5% B, 18 min 80% B, 19 min 90% B. The Q-exactive plus spectrometer completely controlled by the Xcalibur software (Thermo Scientific) was operating in electrospray positive mode. Typical electrospray ionization conditions were as follows: electrospray voltage 4 kV; capillary temperature 320 °C, probe temperature 325 °C, sheath gas flow 40 U, and auxiliary gas 10 U. The MS scan was acquired in the 400 to 1900 m/z range with the resolution set to 140,000. Data analysis was performed with Biopharma Finder 3.2 and intact protein spectra were automatically deconvoluted with Default-Auto Xtract.

CD spectroscopy

The protein (4 μM) was dialyzed against potassium phosphate fluoride buffer (10 mM KH_2PO_4, 100 mM KF, 0.1 mM DTT) and then supplemented with sonicated PC(18:1/18:1) liposomes at increasing concentration in a quartz cell with an optical path length of 0.05 cm. CD spectra were measured at RT in a Jasco J-815 CD spectrometer at a scan speed of 50 nm/min from 195 to 260 nm. For each condition, five spectra were accumulated and corrected for the blank, which was recorded under the same conditions in the absence of protein. Estimation of the percentage of α-helix was performed using the CD analysis and plotting tool CAPITO.

Fluorescence experiments

All fluorescence experiments were performed in a Jasco FP 8300 fluorimeter using a cylindrical cuvette (volume 600 μl) equipped with a stir bar and thermostated at 37 °C. For NBD fluorescence, excitation was set at 500 nm (bandwidth 1 nm) and emission was recorded from 520 to 650 nm (bandwidth 10 nm). For tryptophan fluorescence, excitation was set at 295 nm (bandwidth 2.5 nm) and emission was recorded from 305 to 450 nm (bandwidth 5 nm). Fluorescence energy transfer between TPD54 tryptophans and DPH-PC was measured by exciting tryptophan at 280 nm (bandwidth 1 nm) and following the emission of DPH-PC at 460 nm (bandwidth 5 nm) over time. The cuvette initially contained HKM buffer (Hepes 50 mM, pH 7.2, K acetate 120 mM, $MgCl_2$ 1 mM, DTT 1 mM). For NBD fluorescence, 0.1 μM NBD-labeled TPD54 was added, followed by liposomes of defined size and composition. For tryptophan fluorescence, 0.1 μM unlabeled TPD54 was added, followed by liposomes of defined size and composition. Emission spectra were recorded after each addition and were corrected for the corresponding blank, that is, a similar buffer/liposome mixture in the absence of protein.

Cell culture, protein expression, and antibodies

hTERT-RPE1 cells from ATCC were cultured in Dulbecco's modified Eagle's medium/F12 medium with glutaMAX (Gibco) containing 10% serum, 1% antibiotics (Zell Shield, Minerva Biolabs) and were incubated in a 5% CO_2 humidified atmosphere at 37 °C. Cells were seeded on μDish or μSlide (Ibidi). Plasmids were transfected using Lipofectamine 3000 reagent according to the instruction's guidelines (Thermo Fisher Scientific). After 6 h, the cells were fixed with paraformaldehyde 4% for 20 min at RT. Golgi staining was performed using sheep polyclonal antibody against TGN46 (AHP500G, Bio-Rad).

Live cell observations for FRAP experiments were done using a confocal microscope (Zeiss LSM-780). Images were analyzed using Fiji J software (Fiji).

To determine the fraction of GFP-TPD54 and mutants at the Golgi, we outlined the Golgi area from the TGN46 signal carried out in the red channel. Then, we applied the corresponding mask to the green channel to define a region of interest (ROI) at the Golgi and a ROI of the same area in the cytosol. Once the background was subtracted, we determined the average fluorescence in each ROI and calculated the Golgi/cytosol ratio. All images were acquired with a confocal microscope and were analyzed using Volocity software (Volocity).

For STED experiments, TPD-54 and ALPS(GMAP-210)-ACC1 were cloned in the halo-tag vectors HTN and HTC, respectively. After transfection, these constructs were revealed using a Janelia Fluor 549 ligand (Promega). Endogeneous proteins were labeled with Rb polyclonal antibody anti-TPD52L2 (ProteinTech), Rb polyclonal antibody anti-GMAP-210 (ProteinTech), or Ms monoclonal anti-Trip230 human (Invitrogen). Images were acquired on a Leica confocal TCS SP8 STED microscope. Deconvolution was performed using Huygens Professional software (Scientific Volume Imaging).

Data availability

All data are contained within the article and the supporting information.

Supporting information—Supplemental Tables S1–S2 and Figures S1–S3. This article contains supporting information.

Acknowledgments—We thank S Miserey (institute Curie), G Lenoir (Université Paris Saclay), and all lab members for support and helpful discussions. This work was supported by the Agence Nationale de la Recherche (ANR Grant # 195624, Vesicle Filtering).

Author contributions—A. R., M. M., and B. A. conceptualization; A. R., M. M., S. A., A. S. G., A. P., and D. D. methodology; A. R. and M. M. formal analysis; A. R. and M. M. investigation; A. R., M. M., S. A., A. S. G., and D. D. data curation; B. A. writing–original draft; A. R., M. M., S. A., A. S. G., A. P., D. D., and B. A. writing–review & editing; A. R. and M. M. visualization; B. A. supervision; B. A. funding acquisition.

Conflict of interest—The authors declare that they have no conflicts of interest with the contents of this article.

Abbreviations—The abbreviations used are: AH, amphipathic helix; ALPS, amphipathic lipid packing sensor; DPH-PC, diphenylhexatriene PC; FRAP, fluorescence recovery after photo bleaching; GA, Golgi apparatus; MS, mass spectrometry; MW, molecular weight; NBD, nitrobenzoxadiazole; PC, phosphatidylcholine; PS, phosphatidylserine; STED, stimulated emission-depletion; TGN, *trans*-Golgi network.

References

1. Bonifacino, J. S., and Glick, B. S. (2004) The mechanisms of vesicle budding and fusion. *Cell* **116**, 153–166
2. Hurley, J. H., Boura, E., Carlson, L.-A., and Różycki, B. (2010) Membrane budding. *Cell* **143**, 875–887
3. Dell'Angelica, E. C., and Bonifacino, J. S. (2019) Coatopathies: genetic disorders of protein coats. *Annu. Rev. Cell Dev. Biol.* **35**, 131–168
4. Lee, M. C. S., Miller, E. A., Goldberg, J., Orci, L., and Schekman, R. (2004) Bi-directional protein transport between the ER and Golgi. *Annu. Rev. Cell Dev. Biol.* **20**, 87–123
5. Barlowe, C. (1994) COPII: a membrane coat formed by sec proteins that drive vesicle budding from the endoplasmic reticulum. *Cell* **77**, 895–907
6. Malhotra, V., Serafini, T. A., Orci, L., Shepherd, J. C., and Rothman, J. E. (1989) Purification of a novel class of coated vesicles mediating biosynthetic protein transport through the Golgi stack. *Cell* **58**, 329–336
7. McCaughey, J., and Stephens, D. J. (2019) ER-to-golgi transport: a sizeable problem. *Trends Cell Biol.* **29**, 940–953
8. Hutchings, J., and Zanetti, G. (2019) Coat flexibility in the secretory pathway: a role in transport of bulky cargoes. *Curr. Opin. Cell Biol.* **59**, 104–111
9. Yamamoto, H., Kakuta, S., Watanabe, T. M., Kitamura, A., Sekito, T., Kondo-Kakuta, C., *et al.* (2012) Atg9 vesicles are an important membrane source during early steps of autophagosome formation. *J. Cell Biol.* **198**, 219–233
10. Kishi-Itakura, C., Koyama-Honda, I., Itakura, E., and Mizushima, N. (2014) Ultrastructural analysis of autophagosome organization using mammalian autophagy-deficient cells. *J. Cell Sci.* **127**, 4089–4102
11. Larocque, G., La-Borde, P. J., Clarke, N. I., Carter, N. J., and Royle, S. J. (2019) Tumor protein D54 defines a new class of intracellular transport vesicles. *J. Cell Biol.* **219**, e201812044
12. Boutros, R., Fanayan, S., Shehata, M., and Byrne, J. A. (2004) The tumor protein D52 family: many pieces, many puzzles. *Biochem. Biophys. Res. Commun.* **325**, 1115–1121
13. Giménez-Andrés, M., Čopič, A., and Antonny, B. (2018) The many faces of amphipathic helices. *Biomolecules* **8**, 45
14. Drin, G., and Antonny, B. (2010) Amphipathic helices and membrane curvature. *FEBS Lett.* **584**, 1840–1847
15. Drin, G., Casella, J.-F., Gautier, R., Boehmer, T., Schwartz, T. U., and Antonny, B. (2007) A general amphipathic alpha-helical motif for sensing membrane curvature. *Nat. Struct. Mol. Biol.* **14**, 138–146
16. Magdeleine, M., Gautier, R., Gounon, P., Barelli, H., Vanni, S., and Antonny, B. (2016) A filter at the entrance of the Golgi that selects vesicles according to size and bulk lipid composition. *eLife* **5**, 292
17. Bigay, J., Casella, J.-F., Drin, G., Mesmin, B., and Antonny, B. (2005) ArfGAP1 responds to membrane curvature through the folding of a lipid packing sensor motif. *EMBO J.* **24**, 2244–2253
18. Vanni, S., Vamparys, L., Gautier, R., Drin, G., Etchebest, C., Fuchs, P. F. J., *et al.* (2013) Amphipathic lipid packing sensor motifs: probing bilayer defects with hydrophobic residues. *Biophys. J.* **104**, 575–584
19. van Hilten, N., Stroh, K. S., and Risselada, H. J. (2020) Membrane thinning induces sorting of lipids and the amphipathic lipid packing sensor (ALPS) protein motif. *Front. Physiol.* **11**, 250
20. Vamparys, L., Gautier, R., Vanni, S., Bennett, W. F. D., Tieleman, D. P., Antonny, B., *et al.* (2013) Conical lipids in flat bilayers induce packing defects similar to that induced by positive curvature. *Biophys. J.* **104**, 585–593
21. Vanni, S., Hirose, H., Barelli, H., Antonny, B., and Gautier, R. (2014) A sub-nanometre view of how membrane curvature and composition modulate lipid packing and protein recruitment. *Nat. Commun.* **5**, 4916
22. Antonny, B. (2011) Mechanisms of membrane curvature sensing. *Annu. Rev. Biochem.* **80**, 101–123
23. Mesmin, B., Drin, G., Levi, S., Rawet, M., Cassel, D., Bigay, J., *et al.* (2007) Two lipid-packing sensor motifs contribute to the sensitivity of ArfGAP1 to membrane curvature. *Biochemistry* **46**, 1779–1790
24. Ambroggio, E. E., Sorre, B., Bassereau, P., Goud, B., Manneville, J.-B., and Antonny, B. (2010) ArfGAP1 generates an Arf1 gradient on continuous lipid membranes displaying flat and curved regions. *EMBO J.* **29**, 292–303
25. Zendeh-boodi, Z., Yamamoto, T., Sakane, H., and Tanaka, K. (2013) Identification of a second amphipathic lipid-packing sensor-like motif that contributes to Gcs1p function in the early endosome-to-TGN pathway. *J. Biochem.* **153**, 573–587
26. Xu, P., Baldridge, R. D., Chi, R. J., Burd, C. G., and Graham, T. R. (2013) Phosphatidylserine flipping enhances membrane curvature and negative charge required for vesicular transport. *J. Cell Biol.* **202**, 875–886
27. Drin, G., Morello, V., Casella, J.-F., Gounon, P., and Antonny, B. (2008) Asymmetric tethering of flat and curved lipid membranes by a golgin. *Science* **320**, 670–673
28. Sato, K., Roboti, P., Mironov, A. A., and Lowe, M. (2015) Coupling of vesicle tethering and Rab binding is required for *in vivo* functionality of the golgin GMAP-210. *Mol. Biol. Cell.* **26**, 537–553
29. Cabrera, M., Langemeyer, L., Mari, M., Rethmeier, R., Orban, I., Perz, A., *et al.* (2010) Phosphorylation of a membrane curvature-sensing motif switches function of the HOPS subunit Vps41 in membrane tethering. *J. Cell Biol.* **191**, 845–859
30. Ho, R., and Stroupe, C. (2016) The HOPS/class C Vps complex tethers high-curvature membranes *via* a direct protein-membrane interaction. *Traffic* **17**, 1078–1090
31. Krabben, L., Fassio, A., Bhatia, V. K., Pechstein, A., Onofri, F., Fadda, M., *et al.* (2011) Synapsin I senses membrane curvature by an amphipathic lipid packing sensor motif. *J. Neurosci.* **31**, 18149–18154
32. Moser von Filseck, J., Vanni, S., Mesmin, B., Antonny, B., and Drin, G. (2015) A phosphatidylinositol-4-phosphate powered exchange mechanism to create a lipid gradient between membranes. *Nat. Commun.* **6**, 6671
33. Monje-Galvan, V., and Klauda, J. B. (2018) Preferred binding mechanism of Osh4's amphipathic lipid-packing sensor motif, insights from molecular dynamics. *J. Phys. Chem. B* **122**, 9713–9723
34. Brier, L. W., Ge, L., Stjepanovic, G., Thelen, A. M., Hurley, J. H., and Schekman, R. (2019) Regulation of LC3 lipidation by the autophagy-specific class III phosphatidylinositol-3 kinase complex. *Mol. Biol. Cell.* **30**, 1098–1107

35. Fan, W., Nassiri, A., and Zhong, Q. (2011) Autophagosome targeting and membrane curvature sensing by Barkor/Atg14(L). *Proc. Natl. Acad. Sci. U. S. A.* **108**, 7769–7774
36. Ohashi, Y., Tremel, S., Masson, G. R., McGinney, L., Boulanger, J., Rostislavleva, K., *et al.* (2020) Membrane characteristics tune activities of endosomal and autophagic human VPS34 complexes. *eLife* **9**, e58281
37. Mesmin, B., Bigay, J., Polidori, J., Jamecna, D., Lacas-Gervais, S., and Antonny, B. (2017) Sterol transfer, PI4P consumption, and control of membrane lipid order by endogenous OSBP. *EMBO J.* **36**, 3156–3174
38. Nordeen, S. A., Turman, D. L., and Schwartz, T. U. (2020) Yeast Nup84-Nup133 complex structure details flexibility and reveals conservation of the membrane anchoring ALPS motif. *Nat. Commun.* **11**, 6060
39. Sathasivam, P., Bailey, A. M., Crossley, M., and Byrne, J. A. (2001) The role of the coiled-coil motif in interactions mediated by TPD52. *Biochem. Biophys. Res. Commun.* **288**, 56–61
40. Tunyasuvunakool, K., Adler, J., Wu, Z., Green, T., Zielinski, M., Žídek, A., *et al.* (2021) Highly accurate protein structure prediction for the human proteome. *Nature* **596**, 590–596
41. Gautier, R., Douguet, D., Antonny, B., and Drin, G. (2008) HELIQUEST: a web server to screen sequences with specific alpha-helical properties. *Bioinformatics* **24**, 2101–2102
42. Wong, M., and Munro, S. (2014) Membrane trafficking. The specificity of vesicle traffic to the Golgi is encoded in the golgin coiled-coil proteins. *Science* **346**, 1256898
43. Garten, M., Prévost, C., Cadart, C., Gautier, R., Bousset, L., Melki, R., *et al.* (2015) Methyl-branched lipids promote the membrane adsorption of α-synuclein by enhancing shallow lipid-packing defects. *Phys. Chem. Chem. Phys.* **17**, 15589–15597
44. Rath, A., Glibowicka, M., Nadeau, V. G., Chen, G., and Deber, C. M. (2009) Detergent binding explains anomalous SDS-PAGE migration of membrane proteins. *Proc. Natl. Acad. Sci. U. S. A.* **106**, 1760–1765
45. Wiedemann, C., Bellstedt, P., and Görlach, M. (2013) CAPITO–a web server-based analysis and plotting tool for circular dichroism data. *Bioinformatics* **29**, 1750–1757
46. Antonny, B., Béraud-Dufour, S., Chardin, P., and Chabre, M. (1997) N-terminal hydrophobic residues of the G-protein ADP-ribosylation factor-1 insert into membrane phospholipids upon GDP to GTP exchange. *Biochemistry* **36**, 4675–4684
47. Jamecna, D., Polidori, J., Mesmin, B., Dezi, M., Levy, D., Bigay, J., *et al.* (2019) An intrinsically disordered region in OSBP acts as an entropic barrier to control protein dynamics and orientation at membrane contact sites. *Dev. Cell* **49**, 220–234.e8
48. Pranke, I. M., Morello, V., Bigay, J., Gibson, K., Verbavatz, J. M., Antonny, B., *et al.* (2011) Synuclein and ALPS motifs are membrane curvature sensors whose contrasting chemistry mediates selective vesicle binding. *J. Cell Biol.* **194**, 89–103
49. Horchani, H., de Saint-Jean, M., Barelli, H., and Antonny, B. (2014) Interaction of the Spo20 membrane-sensor motif with phosphatidic acid and other anionic lipids, and influence of the membrane environment. *PLoS One* **9**, e113484
50. Mayer, L. D., Hope, M. J., and Cullis, P. R. (1986) Vesicles of variable sizes produced by a rapid extrusion procedure. *Biochim. Biophys. Acta* **858**, 161–168
51. Olson, F., Hunt, C. A., Szoka, F. C., Vail, W. J., and Papahadjopoulos, D. (1979) Preparation of liposomes of defined size distribution by extrusion through polycarbonate membranes. *Biochim. Biophys. Acta* **557**, 9–23
52. Hatzakis, N. S., Bhatia, V. K., Larsen, J., Madsen, K. L., Bolinger, P.-Y., Kunding, A. H., *et al.* (2009) How curved membranes recruit amphipathic helices and protein anchoring motifs. *Nat. Chem. Biol.* **5**, 835–841
53. Jensen, M. B., Bhatia, V. K., Jao, C. C., Rasmussen, J. E., Pedersen, S. L., Jensen, K. J., *et al.* (2011) Membrane curvature sensing by amphipathic helices: a single liposome study using α-synuclein and annexin B12. *J. Biol. Chem.* **286**, 42603–42614
54. Tian, A., and Baumgart, T. (2009) Sorting of lipids and proteins in membrane curvature gradients. *Biophys. J.* **96**, 2676–2688
55. Wong, M., Gillingham, A. K., and Munro, S. (2017) The golgin coiled-coil proteins capture different types of transport carriers *via* distinct N-terminal motifs. *BMC Biol.* **15**, 3
56. Larocque, G., Moore, D. J., Sittewelle, M., Kuey, C., Hetmanski, J. H. R., La-Borde, P. J., *et al.* (2021) Intracellular nanovesicles mediate α5β1 integrin trafficking during cell migration. *J. Cell Biol.* **220**, e202009028
57. Zhang, L., Wang, Y., Dong, Y., Pant, A., Liu, Y., Masserman, L., *et al.* (2022) The endophilin curvature-sensitive motif requires electrostatic guidance to recycle synaptic vesicles *in vivo*. *Dev. Cell* **57**, 750–766.e5
58. Jao, C. C., Hegde, B. G., Chen, J., Haworth, I. S., and Langen, R. (2008) Structure of membrane-bound alpha-synuclein from site-directed spin labeling and computational refinement. *Proc. Natl. Acad. Sci. U. S. A.* **105**, 19666–19671
59. Knowles, D. G., Lee, J., Taneva, S. G., and Cornell, R. B. (2019) Remodeling of the interdomain allosteric linker upon membrane binding of CCT α pulls its active site close to the membrane surface. *J. Biol. Chem.* **294**, 15531–15543
60. Ishida, T., and Kinoshita, K. (2007) PrDOS: prediction of disordered protein regions from amino acid sequence. *Nucl. Acids Res.* **35**. https://doi.org/10.1093/nar/gkm363
61. Xue, B., Dunbrack, R. L., Williams, R. W., Dunker, A. K., and Uversky, V. N. (2010) PONDR-FIT: a meta-predictor of intrinsically disordered amino acids. *Biochim. Biophys. Acta* **1804**, 996–1010
62. Erdős, G., Pajkos, M., and Dosztányi, Z. (2021) IUPred3: prediction of protein disorder enhanced with unambiguous experimental annotation and visualization of evolutionary conservation. *Nucl. Acids Res.* **49**, W297–W303
63. Hu, G., Katuwawala, A., Wang, K., Wu, Z., Ghadermarzi, S., Gao, J., *et al.* (2021) flDPnn: accurate intrinsic disorder prediction with putative propensities of disorder functions. *Nat. Commun.* **12**, 4438
64. Lupas, A., Van Dyke, M., and Stock, J. (1991) Predicting coiled coils from protein sequences. *Science* **252**, 1162–1164
65. Goedhart, J. (2021) SuperPlotsOfData-a web app for the transparent display and quantitative comparison of continuous data from different conditions. *Mol. Biol. Cell.* **32**, 470–474